

# Polar nephelometer based on a rotational confocal imaging setup

Jean-Luc Castagner and Irving J. Bigio

Rapid measurement of the angular distribution of light scattered by particles, the scattering phase function, is achieved by using a new type of polar nephelometer, a device for measuring the angular scattered-light intensity distribution, with a high angular precision and across many orders of magnitude of intensity. The design offers high-speed measurements and avoids many of the problems often associated with traditional goniometers when they are used for measurements of light scattering from small particles or biological cells in suspension. Our system relies on confocal imaging of the test space with off-axis parabolas, using a rotating mirror to scan the angular field of view at the second focus of a pair of conjugated parabolic mirrors, with the test space located at the first focus. The angular resolution of the system is limited mainly by the data-acquisition sampling frequency. In this proof-of-principle demonstration the system performs multiple scans of a 55 deg field of view in a very short time ( $<1$  s). To significantly increase the signal-to-noise ratio, we averaged the successively acquired scans during this time. Polystyrene spheres dispersed in water at low concentrations were used to test the system. The scattering patterns obtained were found to be in good agreement with Mie theory calculations. © 2006 Optical Society of America

OCIS codes: 120.5820, 290.0290.

## 1. Introduction

The topic of light scattering by particles has been widely investigated for more than a century. There is significant interest in this topic, as it has applications in a wide number of areas such as astronomy, biology, combustion, pollution control, atmospheric physics, etc. The most commonly used description of light scattering by homogeneous spherical particles is Mie theory, developed by Gustave Mie in 1908. However, it is speculated that Debye or Lorenz was first to formulate this problem.<sup>1</sup> This theory effectively describes the exact solution to the scattering of a plane wave by a homogeneous sphere.

Experimentally, the angular measurement of light scattered from an individual particle or an ensemble of particles aims at determining particle size, refractive index, and shape by using an appropriate light-

scattering theory. This is of importance, for example, in radiative transfer and climate modeling. Polar nephelometers have been specifically designed for measuring aerosol properties.<sup>2-4</sup> Additionally, various theories have been developed to tackle the problems of light scattering by multilayered spherical particles,<sup>5,6</sup> nonspherical particles,<sup>5-12</sup> particles with inclusions,<sup>13,14</sup> inhomogeneous particles,<sup>9</sup> and ensembles of particles.<sup>5,15-17</sup>

Commonly, a polar nephelometer system is based on a goniometric system that invokes the rotation of a light-intensity detector around a test space illuminated by a static beam of collimated light. In this configuration mechanical constraints render the dynamic of the measurement process very slow. In the case in which few particles are in motion through the test space, the only possibility to gain an estimation of the phase function is to use multiple fixed detectors at different angles,<sup>3</sup> allowing almost instantaneous measurements. However, the geometric and operating complexities of such systems render the task of single-particle characterization challenging, using expensive systems that are less adaptable and also limited in their angular resolution.

In this paper we present a new polar nephelometer system based on confocal imaging of the test space by using a rotating mirror to scan the angular field of view at the second focus of a pair of conjugated par-

---

The authors are with Boston University, 44 Cummington Street, Boston, Massachusetts 02215. J.-L. Castagner (jlcastagner@hotmail.com) is with the Department of Biomedical Engineering, and I. J. Bigio (bigio@bu.edu) is with the Departments of Biomedical Engineering and of Electrical and Computer Engineering.

Received 14 September 2005; revised 30 November 2005; accepted 1 December 2005; posted 7 December 2005 (Doc. ID 64750).

0003-6935/06/102232-08\$15.00/0

© 2006 Optical Society of America

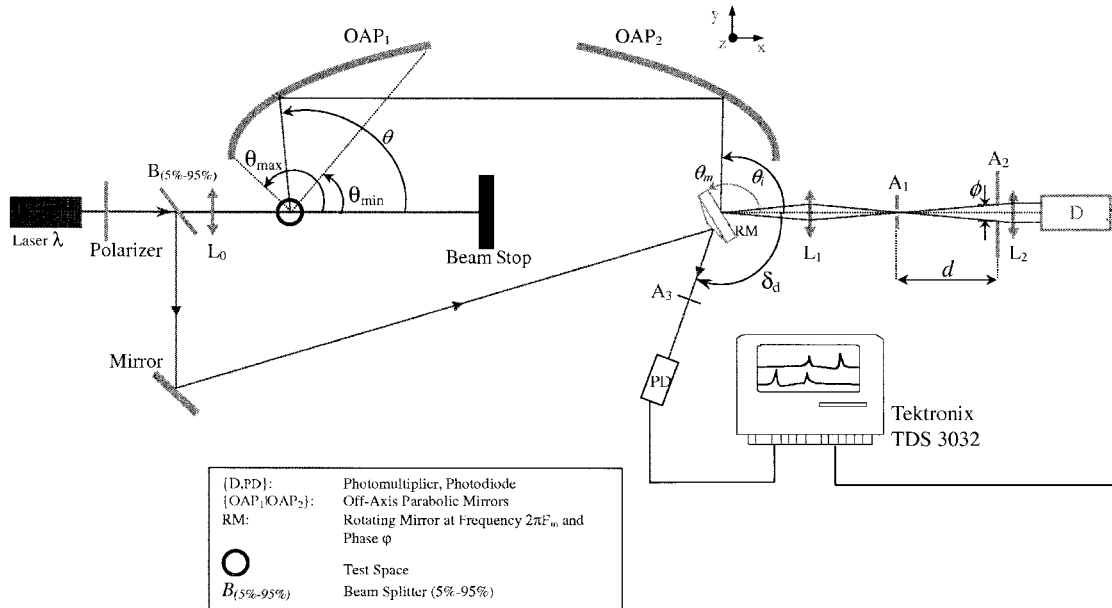


Fig. 1. Setup of the polar nephelometer.

abolic mirrors, with the test space located at the first focus. This system's advantages are found in its wide dynamic range of measurement and its capacity to perform angular scanning of the test space in a short time. Using a statistical treatment of successively acquired scans leads to an improved signal-to-noise ratio (SNR) because this method is inherently insensitive to particle motion or variations in the number of particles in the test space, provided that the speed of angular scanning is fast compared with the particle motion.

We describe the design of the nephelometer in a proof-of-principle demonstration, present the materials used for calibration, and finally discuss the experimental tests carried out and their validity.

## 2. Description of the System

### A. Main Setup

The main setup (see Fig. 1) comprises a polarized He-Ne laser beam ( $\lambda = 632.8$  nm, power = 3 mW) focused through lens  $L_0$  ( $f = 100$  mm) in the test space located at the focus of the first off-axis parabola,  $OAP_1$ . [See Fig. 2 for a schematic diagram of the test space (top view).] Light scattered at angle  $\theta$  is deflected parallel to the  $x$  axis by the first off-axis parabolic mirror  $OAP_1$  ( $90^\circ$ ; 25.4 mm diameter; 12.7 mm parent focal length; protected aluminum surface; from Edmund Optics Inc.). The scattered light is then refocused in the conjugated image of the test space by mirror  $OAP_2$  (identical to  $OAP_1$ ). The OAPs were used in a configuration that allows a field of view from  $\theta_{\min} = 70^\circ$  to  $\theta_{\max} = 125^\circ$ . A greater angular range can be covered simply and quickly by deflecting the laser beam to impinge on the test space from different angles.

The confocal imaging system uses a 1:1 imaging

lens  $L_1$  ( $f = 50.0$  mm), the foci of which are at the axis of rotation of the rotating mirror RM and at the plane of aperture  $A_1$  (diameter  $\phi_{A1} = 0.4$  mm). The RM is mounted on the shaft of a brushless dc motor, with the mirror face on the axis of rotation. Light rays deflected by RM pass successively through  $L_1$ ,  $A_1$ , and aperture  $A_2$ , and they are finally focused by  $L_2$  ( $f = 250$  mm) onto photodetector D (Hamamatsu, Ltd.). Thus, by setting the diameter  $\phi$  of  $A_2$  and the distance  $d$  between  $A_2$  and  $A_1$ , one achieves an angular scan of the test space with a static solid angle of

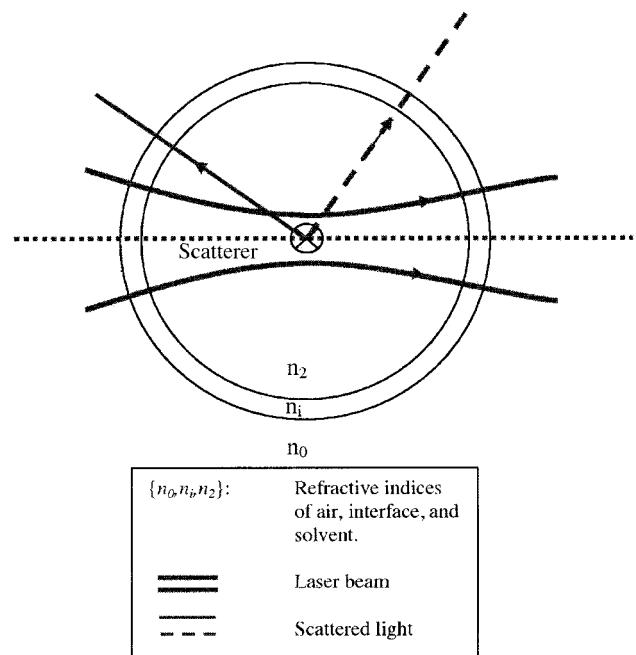


Fig. 2. Schematic diagram of the test space (top view).

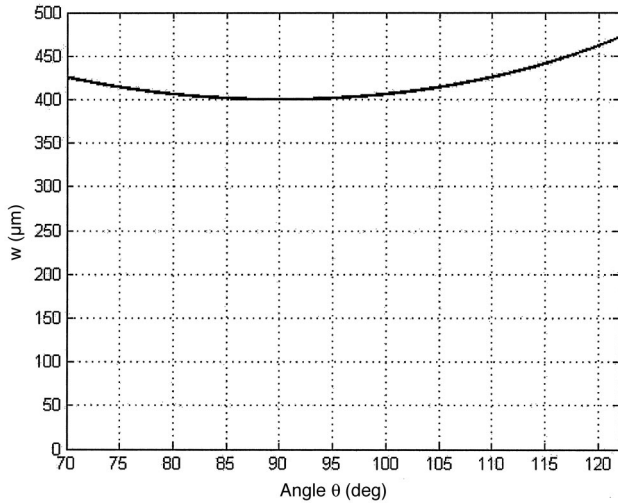


Fig. 3. Calculated variation of the imaged test-space width.

light collection:

$$\Omega = \pi\phi^2/d^2. \quad (1)$$

A beam splitter and mirror deflect a portion ( $\approx 5\%$ ) of the laser beam onto the back face of the RM, on which were mounted two small mirrors at an arbitrary angle of  $22.2^\circ$  to each other, to serve as an angle reference for the acquisition of the scattered-light intensity. A photodiode was used to detect the light reflected from the back mirrors. The resulting signal consisted of two distinct peaks whose positions gave the reference for two angles of the RM. (A servo motor with angle readout would obviate the need for this reference. See discussion in Subsection 2.C.)

For this set of demonstration experiments, the laser polarization was oriented to be *s* polarized (perpendicular to the scattering plane).

The OAPs (Edmund Optics, Inc.) are diamond-turning machined and have poor surface quality at the wavelength of interest (632.8 nm), inducing significant surface diffraction when coherent light is reflected. However, the confocal geometry of the design inherently reduces the effect of this diffraction in a manner similar to the way a confocal microscope rejects out-of-focal-plane light: diffraction induced by the OAP's ruled surface propagates in directions non-parallel to the OAP's collimation axis. This light is therefore eliminated through the confocal setup.

#### B. Confocal Setup

A confocal setup was used to select scattered light originating from the center of the test space. Because aperture  $A_1$  and lens  $L_1$  are fixed, the width  $w(\theta) = \phi_{A1} |\cos(\theta - 90)|$  of the imaged test space depends on the angular position of the RM. Figure 3 shows the calculated variation of the imaged test space width  $w$  with respect to the scattering angle  $\theta$ .

The focusing of the laser beam through a lens leads to the focal-spot diameter  $d_f$  as follows<sup>18</sup>:

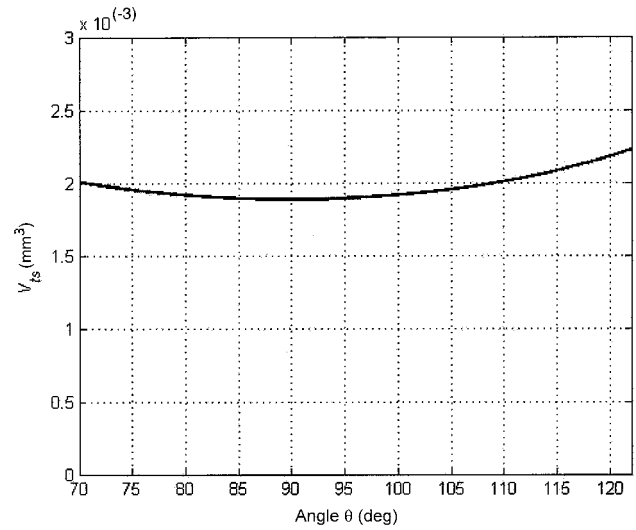


Fig. 4. Calculated variation of the imaged test-space volume.

$$d_f = \frac{2\lambda f}{\pi\sigma_{\text{FWHM}}}. \quad (2)$$

With  $\lambda = 632.8$  nm,  $\sigma_{\text{FWHM}} = 1.5$  mm, and  $f = 100.0$  mm, we find  $d_f \approx 75.6$   $\mu\text{m}$ .

The volume of the test space can be approximated as

$$V_{\text{ts}}(\theta) = w(\theta)\pi(d_f^2/4). \quad (3)$$

Figure 4 shows the calculated variation of  $V_{\text{ts}}$  with respect to the scattering angle  $\theta$ .

#### C. Rotational Imaging

The rotational imaging of the test space is achieved with a face-centered mirror mounted on a simple brushless dc motor. Upon rotation, the mirror reflects the light impinging from the parabolic mirror pair to the detector. Thus a continuous angular scanning of the test space is achieved. In the following discussion, we denote  $\theta$ ,  $\theta_i$ , and  $\theta_m$  as the real scattering angle, the imaged scattering angle, and the mechanical angle of the RM, respectively;  $\delta_D$  refers to the angular orientation of detector D with respect to the axis of the foci. In this configuration we had set  $\delta_D = 0$ . The rotation speed of the RM is designated as a frequency,  $F_m$ . The sampling frequency of the data-acquisition system is  $F_s$ . Therefore the angular resolution of the acquisition system is given by

$$\Delta\theta = \frac{720F_m}{F_s/2}. \quad (4)$$

Note that  $F_s/2$  is used because of the Nyquist criterion for sampling.

The equation of rotation for the RM is given by

$$\theta_m(t) = 360F_m t + \varphi_m, \quad (5)$$

where  $F_m$  is the frequency of rotation of the motor and  $\varphi_m$  is its phase (in degrees).

The rotation of RM induces a change in the deflection angles according to

$$\cos[\theta_i(t)] = \cos[2(360F_m t + \varphi_m)], \quad (6)$$

where  $t$  is the time expressed in seconds. The scattering angle  $\theta$  is expressed as a function of the deflected angle  $\theta_i$  and the relative angle of detector D, namely  $\delta_D$  (not to be confused with  $\delta_d$ ):

$$\theta = 180 - \theta_i + \delta_D. \quad (7)$$

Combining Eqs. (5) and (6) with (7) leads to

$$\theta = 180 - \arccos[2(360F_m t + \varphi_m)] + \delta_D. \quad (8)$$

These equations describe the motion of the rotational imaging of the system. Experimentally, however, in this first demonstration the determination of the position of the RM is achieved with a reference beam whose reflection from the back-positioned small-angle-wedge reflecting surface generates two distinct peaks in the signal generated by the photodiode (PD). This will be further explained in Subsection 2.E. (In future improvements of this system we intend to utilize a dc servo motor with a built-in high-resolution angular-position readout, which would eliminate the need for the separate reference beam.)

#### D. Alignment of the Off-Axis Parabolic Mirrors and Rotating Mirror

Off-axis parabolic mirrors are made of a section of a parabolic form, focusing incident collimated light at a specific point. These mirrors allow one to obtain full access to the focal point. Correct alignment of the off-axis parabolas is a critical and nontrivial procedure for accurate operation of the system. The two OAPS were mounted facing each other on an  $x$ - $y$ - $z$  translation stage so that the OAP<sub>1</sub> focal point is the conjugate image of the OAP<sub>2</sub> focal point. A face-centered rotating mirror was mounted on a precision rotation stage ( $\pm 0.1^\circ$ ) at the OAP<sub>1</sub> focal point, in place of the sample holder, to deflect the focused laser beam onto OAP<sub>1</sub> to facilitate the alignment process. We refer to it as the alignment mirror (AM) in the following discussion. Since the laser beam was focused through lens L<sub>0</sub> onto the surface of the AM and the distance from the axis of rotation of the AM to the parabolic surface of OAP<sub>1</sub> was much greater than the Rayleigh range, we safely assumed that the divergence of the laser beam originated from the AM axis of rotation. Therefore we could position the OAP pair in a very precise manner. Using a ray-tracing approach, one would expect that light emerging from the OAP<sub>1</sub> focal point would be deflected in the direction parallel to the  $x$  axis (see Fig. 1).

The  $z$  position of the  $x$ - $y$ - $z$  translation stage was adjusted by rotating the AM to determine the leverage of the swept laser beam. Leverage parallel to the

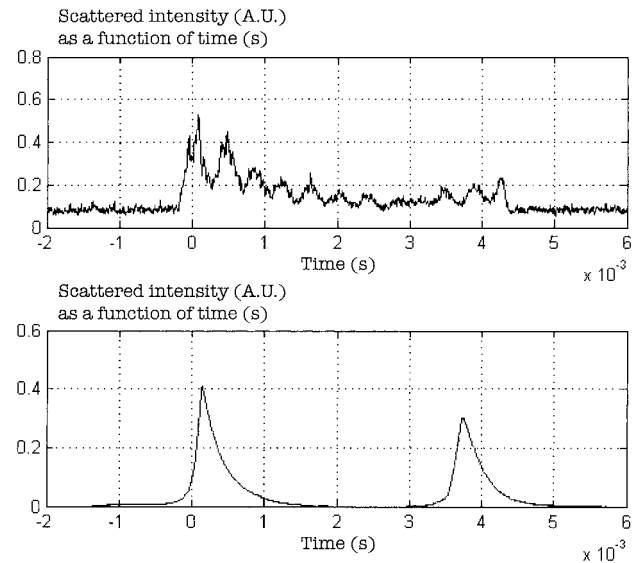


Fig. 5. Angular scan (top) acquired with the trigger reference signal (bottom).

$y$  axis meant that the deflected laser beam was positioned at half-height of the OAP system, in their  $x$ - $y$  plane. Taking the lateral edges of the OAPs as reference points, we iteratively modified the  $x$ - $y$  position of the OAPs until the deflected focused laser beam was propagating parallel to the  $x$  axis between the two OAPs for all positions of the AM. This method has proved to be the most efficient; however, some uncertainty has to be accounted for, as the area of incidence of the laser beam on OAP<sub>2</sub> is larger than on OAP<sub>1</sub> owing to the divergence of the focused laser beam.

The RM was mounted on an  $x$ - $y$  translation stage. When the RM rotates, the laser beam deflected by OAP<sub>2</sub> and incident on RM is swept across the  $x$ - $y$  plane. The alignment of the mirrored surface of the RM to the focal point of OAP<sub>2</sub> was achieved when the laser spot on the mirror surface (due to the weak diffuse scattering of the surface) was visually observed to be static upon rotation of the AM.

When making measurements on a suspension of particles in water, we centered the cylindrical glass tube containing the sample on the axis of the rotation stage, which itself is centered on the OAP<sub>1</sub> focal point.

#### E. Calibration of the System's Field of View

For these initial experiments a small fraction of the laser beam was deflected onto the back surface of the RM, on which were mounted a pair of thin, small mirrors at a wedge angle of  $22.2^\circ$  from each other. Thus, when set into motion, these mirrors deflected the reference beam, generating two distinct signal peaks at detector PD, the position of which was calibrated by using the AM and the focused laser beam. The rotation stage gave the two mechanical angle values corresponding to the reference peak positions. Using Eq. (7) with  $\theta_i = 2\theta_{AM}$  (where  $\theta_{AM}$  is the angular position of the AM relative to the laser beam), we find

(with  $\delta_D = 0^\circ$ ) the following expression for  $\theta$ :

$$\theta = 180 - 2\theta_{AM}. \quad (9)$$

Following this procedure, we were able to match the original signal from photomultiplier D [which was a function of time (in seconds)] with the scattering angle  $\theta$ . Figure 5 shows the angular scan with the reference beam signal.

#### F. Multiple-Scan Measurement Procedure

The measurements were carried out in the following manner. Using the reference signal as an external trigger for the oscilloscope, we acquired and averaged  $N$  successive scans. This yielded a SNR increase of a factor  $\sqrt{N}$ . Given that the dynamics of the scatterers were slow compared with the acquisition time of all signals, the number of acquired scans could be set on the oscilloscope to change the SNR (namely, 1, 2, 4, 8, 16, 32, 64, 128, 256, or 512). For the experimental results presented here,  $N$  was set to 16. Therefore a SNR improvement of a factor of 4 was achieved. Thus three parameters—the speed of rotation of the RM, the intensity of the illumination source, and  $N$ —are interrelated in obtaining the desired SNR.

The addition of successive multiple scans is responsible for the enhanced dynamic range of this method. In conventional goniometer-based measurements, if measurement parameters are set for sufficient SNR at larger scattering angles, then the detector is often saturated by the much-stronger near-forward scattering at smaller angles. This is usually dealt with by varying the integration times at different angles or by adding attenuating filters for the near-forward angles. With our method, the measurement parameters are simply set so that the strongest (near-forward) signal does not saturate, and then the SNR for the weakest signals is enhanced by mathematically adding multiple scans. [Instead of the digital oscilloscope used in this initial demonstration, an automated measurement procedure without restrictions in the values of  $N$  (for example, an analog-to-digital converter with LabVIEW 7.0) would provide a greater flexibility in the system. However, for the angle range of these experiments, setting  $N = 16$  resulted in a sufficiently low-noise level.]

#### G. Particle-Size Distributions

Nonabsorbing polystyrene spheres [certified by the National Institute of Standards and Technology (NIST) and manufactured by Duke Scientific Corp.] with an index of refraction of 1.58 at a wavelength of 632.8 nm were used to test the system. The modal diameters of the size distributions were 2.0, 2.9, 5.01, 6.992, and 8.956  $\mu\text{m}$ , with a standard deviation of 4%, 5%, 1%, 1%, and 1%, respectively (NIST certificates provided by the manufacturer). Low concentrations of each of the size distributions were prepared with distilled water in standard glass test tubes (diameter of 12.7 mm).

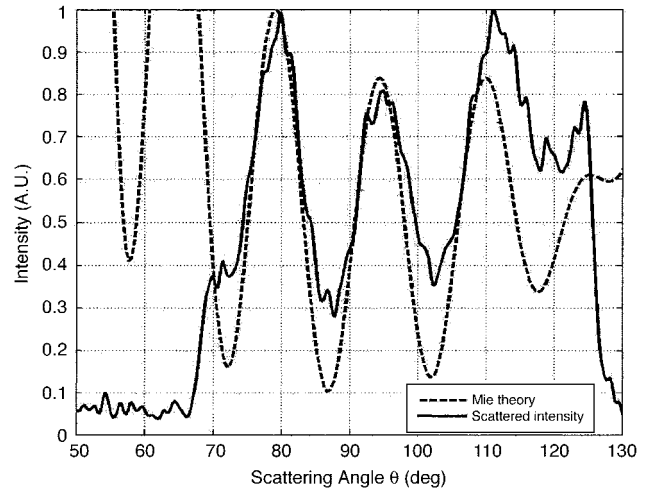


Fig. 6. Scattered intensity (moving average of 50 points, normalized) from sample S1 (2.0  $\mu\text{m}$  modal diameter) particle compared with Mie theory ( $m = 1.58$ ,  $\lambda = 632.8$  nm).

### 3. Results and Discussion

To validate the experimental results, we carried out Mie theory calculations by using a Matlab interface developed by the authors and based on the code from Bohren and Huffman.<sup>19</sup> The theoretical perpendicularly polarized ( $s$ -polarized) component of light scattered by particles from each of the size-distribution modal diameters with refractive index of 1.58 was calculated within the range of scattering angles covered by OAP<sub>1</sub> and were plotted together with the experimental data. In the following discussion we refer to S1, S2, S3, S4, and S5 as the low-concentration samples for size distributions of modal diameters of 2.0, 2.9, 5.01, 6.992, and 8.956  $\mu\text{m}$ , respectively, used in the experiment. Each scattering pattern was obtained by acquiring 16 successive angular scan samples (in less than 1 s) triggered on the reference beam and then averaging them to suppress

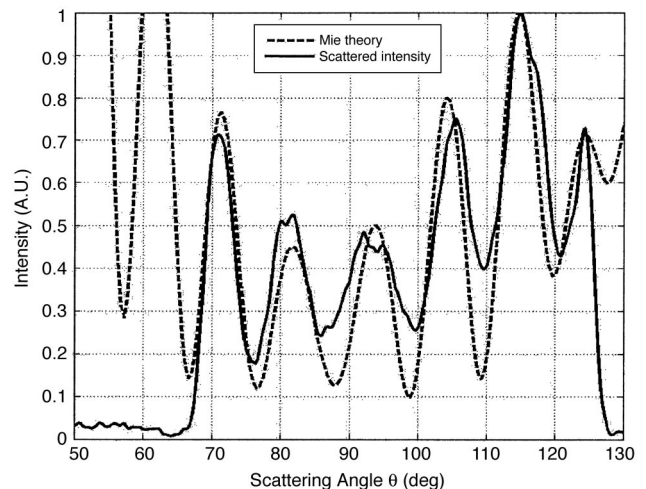


Fig. 7. Scattered intensity (moving average of 50 points, normalized) from sample S2 (2.9  $\mu\text{m}$  modal diameter) particle compared with Mie theory ( $m = 1.58$ ,  $\lambda = 632.8$  nm).

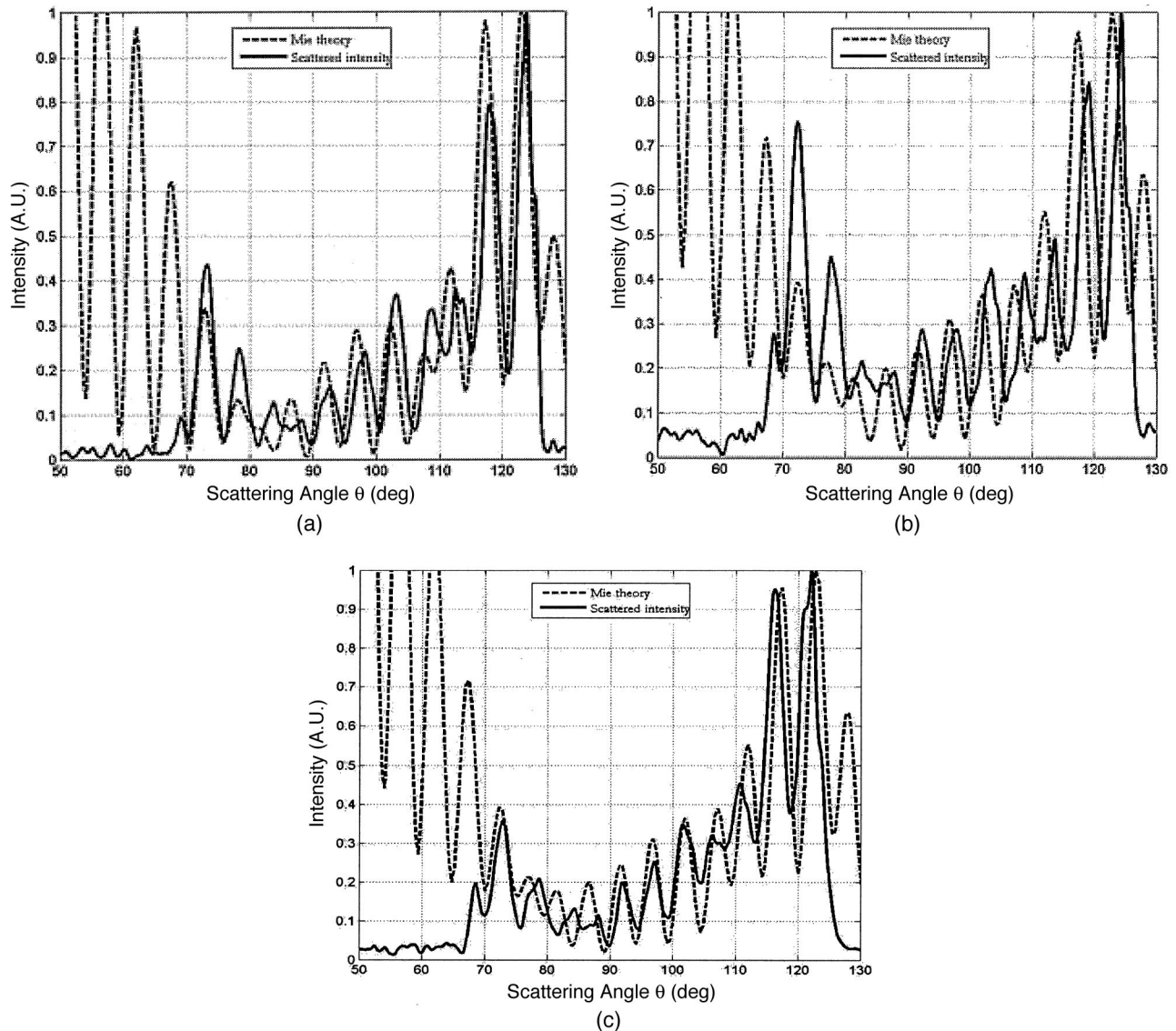


Fig. 8. (a) Scattered intensity (moving average of 50 points, normalized) from sample S3 (5.01  $\mu\text{m}$  modal diameter) particle compared with Mie theory ( $m = 1.58$ ,  $\lambda = 632.8$  nm). (b) Scattered intensity (moving average of 50 points, normalized) from sample S3 (5.01  $\mu\text{m}$  modal diameter) particle compared with Mie theory ( $m = 1.58$ ,  $\lambda = 632.8$  nm). (c) Scattered intensity (moving average of 50 points, normalized) from sample S3 (5.01  $\mu\text{m}$  modal diameter) particle compared with Mie theory ( $m = 1.58$ ,  $\lambda = 632.8$  nm).

uncorrelated signals (e.g., those due to particle motion or photomultiplier noise), thereby significantly increasing the SNR. A smoothing function was applied to further reduce the noise effects without significantly affecting the angular resolution. The results are presented in Figs. 6, 7, 8, 9, and 10 for samples S1, S2, S3, S4, and S5, respectively. In Fig. 8 are shown three different runs [(a), (b), and (c)] to illustrate the discussion points that follow. Each of the traces corresponds to single-scattering signals, as the particles were in low concentrations.

Mie theory calculations were found to be in good agreement with most experimental results. However, discrepancies occurred where the positions of some peaks were shifted from the predicted values [see, for example, Figs. 8(b) and 8(c) and Figs. 9 and 10]. To

explain this phenomenon, we discuss two possible causes:

1. The sample holder used in our experiments was a simple glass test tube with a diameter of 12.7 mm and a thickness of 0.8 mm. It is expected that irregularities in its cylindrical shape, together with the index mismatch between the glass-water and glass-air interfaces and air, can cause slight distortions in the exit angles of scattered light for certain ranges of angles.
2. The samples had standard deviations in their size distributions of, at most, 5%. The size ranges for samples S1, S2, S3, S4, and S5 were 1.92–2.08, 2.76–3.05, 4.96–5.06, 6.92–7.06, and 8.87–9.05  $\mu\text{m}$ , respectively. Therefore it is expected that differences

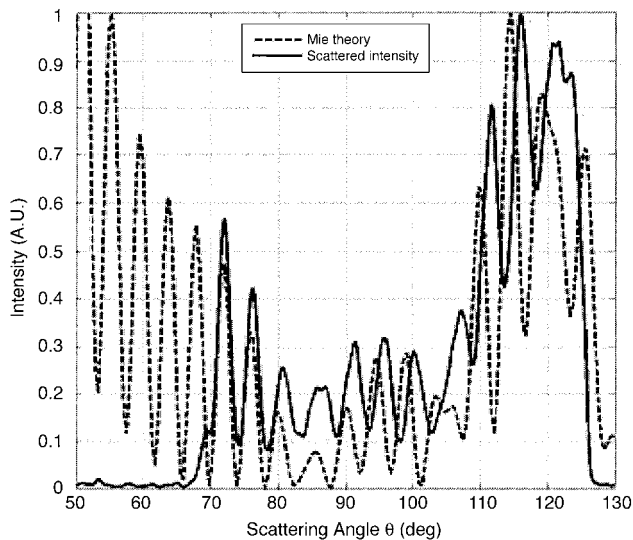


Fig. 9. Scattered intensity (moving average of 50 points, normalized) from sample S4 ( $6.992 \mu\text{m}$  modal diameter) particle compared with Mie theory ( $m = 1.58$ ,  $\lambda = 632.8 \text{ nm}$ ).

from predicted values will occur owing to the slight differences between the modal-diameter value used for the calculations and the actual distributions.

Significant differences in relative amplitudes of the peaks in scattered intensities are also seen in Fig. 8(b). With an angular resolution of  $0.3^\circ$  obtained with aperture  $A_2$ , the smallest peak width of the largest particle size ( $8.956 \mu\text{m}$ ) was clearly resolved. Therefore the difference in amplitudes cannot be accounted for by the angular resolution of the system. Differences between the Mie theory and the measured scattered intensity apparently vary with angle, with greater disparities in either half of the angular

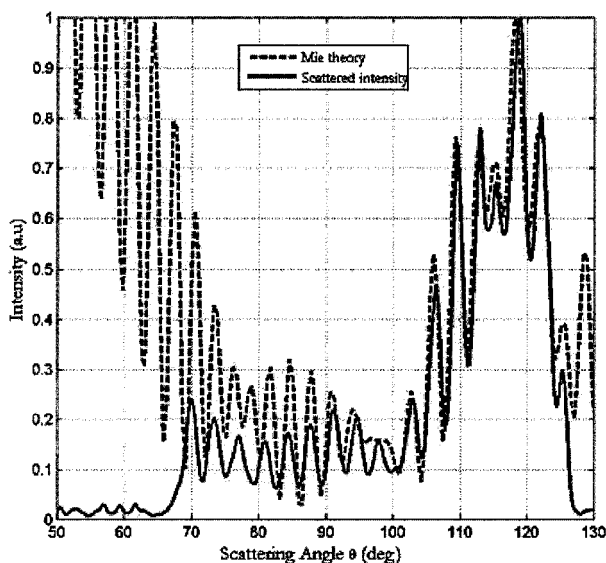


Fig. 10. Scattered intensity (moving average of 50 points, normalized) from sample S5 ( $8.956 \mu\text{m}$  modal diameter) particle compared with Mie theory ( $m = 1.58$ ,  $\lambda = 632.8 \text{ nm}$ ).

field (see also Fig. 10). We believe that this may be due to statistical variations in the small number of large particles in the illumination test volume, resulting in a distorted apparent size distribution.

Another potential source of error that is not specific to the design of our system relates to the nonuniformity of the Gaussian profile of the illuminating laser beam when the particle size is not small compared with the beam-waist diameter. Ideally, the test space should be illuminated with a plane wave of uniform intensity profile. This can be achieved in a number of ways, such as refractive beam-shaping techniques,<sup>20,21</sup> holographic techniques,<sup>22</sup> or beam-sampling techniques.<sup>23</sup>

From the discussion above, we infer that the most likely cause for the discrepancies seen between experimental and predicted data is a possible misalignment or shape distortion of the sample holder at the center of the test space. This leads us to believe that the system can be significantly improved by simple quality control of the component specifications.

#### 4. Conclusion

We have successfully designed and tested a new type of polar nephelometer that allows measurement of a scattering phase function and that has significant benefits over methods that employ stepped goniometers. A rotational confocal imaging was used in conjunction with a pair of conjugated off-axis parabolic mirrors. Tests were carried out on narrow size distributions of polystyrene spheres. Results were in good agreement with Mie theory. We are currently developing a new version of the nephelometer with a more stable rotation system of the rotating mirror, which also does not require the reference beam to calibrate its position. The system will be controlled through a LabVIEW interface and will allow a more effective statistical treatment of the signal. Given the preliminary results presented in this paper, simple improvements of the technique will yield a wider range of particle sizes and angles.

The authors are grateful to Roberto Reif and Ousama A'amar for their comments and suggestions. This research was supported in part by the National Cancer Institute of the National Institutes of Health (grant U54 CA104677).

#### References

1. C. Bohren, and D. Huffman, *Absorption and Scattering of Light by Small Particles* (Wiley-Interscience, 1983).
2. W. Kaller, "A new polar nephelometer for measurement of atmospheric aerosols," *J. Quant. Spectrosc. Radiat. Transf.* **87**, 107–117 (2004).
3. J. F. Gayet, O. Crépel, J. F. Fournol, and S. Oshchepkov, "A new airborne polar nephelometer for the measurements of optical and microphysical cloud properties," *Ann. Geophys.* **15**, 451–459 (1997).
4. F. Li, S. Nyeki, U. Baltensperger, E. Weingartner, M. Lugauer, I. Colbeck, and H. W. Gaggeler, "Aerosol size distribution retrieval from multiwavelength nephelometer data," *J. Aerosol Sci.* **28**, 249–250 (1997).
5. T. Wriedt, "A review of elastic light scattering theories," *Part. Syst. Charact.* **15**, 67–74 (1998).

6. W. Rysakow and M. Ston, "The light scattering by core-mantled sphere," *J. Quant. Spectrosc. Radiat. Transfer* **69**, 121–129 (2001).
7. O. O. Abiola, S. A. Checkley, I. C. Campbell, S. A. Whatley, M. I. Mishchenko, L. D. Travis, and D. W. Mackowski, "T-matrix computations of light scattering by nonspherical particles: a review," *J. Quant. Spectrosc. Radiat. Transfer* **55–5**, 535–575 (1996).
8. C. Bockmann and J. Wauer, "Algorithms for the inversion of light scattering data from uniform and non-uniform particles," *Aerosol Sci.* **32**, 49–61 (2001).
9. Y. Eremin and V. Ivakhnenkos, "Modelling of light scattering by non-spherical inhomogeneous particles," *J. Quantit. Spectrosc. Radiat. Transfer* **60–3**, 475–482 (1998).
10. A. Quirantes, "Light scattering properties of spheroidal coated particles in random orientation," *J. Quant. Spectrosc. Radiat. Transfer* **63**, 263–275 (1999).
11. N. V. Voshchinnikov, "Electromagnetic scattering by homogeneous and coated spheroids: calculations using the separation of variables method," *J. Quant. Spectrosc. Radiat. Transfer* **55–5**, 627–636 (1996).
12. A. Quirantes, A. V. Delgado, "scattering cross sections of randomly oriented coated spheroids," *Journal of Quantitative Spectroscopy and Radiative Transfer* **70**, 261–272 (2001).
13. R. Shuh and T. Wriedt, "Computer programs for light scattering by particles with inclusions," **70**, 715–723 (2001).
14. L. Wind, L. Hofer, A. Nagy, P. Winkler, A. Vrtala, and W. W. Szymanski, "Light scattering from droplets with inclusions and the impact on optical measurement of aerosols," *J. Aerosol Sci.* **35**, 1173–1188 (2004).
15. A. Quirantes, F. Arroyo, and J. Quirantes-Ros, "Multiple light scattering by spherical particle systems and its dependence on concentration: a T-matrix study," *J. Colloid Interface Sci.* **240**, 78–82 (2001).
16. J. C. Auger, B. Stout, and J. Lafait, "Dependent light scattering in dense heterogeneous media," *Physica B* **279**, 21–24 (2000).
17. A. da Silva, C. Andraud, E. Charron, B. Stout, and J. Lafait, "Multiple light scattering in multilayered media: theory, experiments," *Physica B* **338**, 74–78 (2003).
18. Saleh B. E. A. and M. C. Teich, *Fundamentals of Photonics* (Wiley-Interscience, 1991), p. 95.
19. C. F. Bohren and D. R. Huffman, *Absorption and Scattering of Light by Small Particles* (Wiley, 1998), pp. 479–481.
20. J. A. Hoffnagle and C. M. Jefferson, "Design and performance of a refractive optical system that converts a Gaussian to a flattop beam," *Appl. Opt.* **39**, 5488–5499 (2000).
21. X. Tan, G. Ben-Yuan, Y. Guo-Zhen, and D. Bi-Zhen, "Diffractive phase elements for beam shaping: a new design method," *Appl. Opt.* **34**, 1314–1320 (1995).
22. M. Quintanilla and A. M. de Frutos, "Holographic filter that transforms a Gaussian into a uniform beam," *Appl. Opt.* **20**, 879–880 (1981).
23. I. A. Al-Saidi, "Using a simple method: conversion of a Gaussian laser beam into a uniform beam," *Opt. Laser Technol.* **33**, 75–79 (2000).